The Astrophysical Journal, 714:699–712, 2010 May 1 doi:10.1088/0004-637X/714/1/699

MOLECULAR GAS IN $z \sim 6$ QUASAR HOST GALAXIES

Ran Wang[1,2,3], Chris L. Carilli[2], R. Neri[4], D. A. Riechers[5,12], Jeff Wagg[2,6], Fabian Walter[7], Frank Bertoldi[8], Karl M. Menten[9], Alain Omont[10], Pierre Cox[4], and Xiaohui Fan[11]
[1] Purple Mountain Observatory, China Academy of Science, No. 2 Beijing West Road, Nanjing 210008, China
[2] National Radio Astronomy Observatory, P. O. Box 0, Socorro, NM 87801, USA
[3] Department of Astronomy, Peking University, Beijing 100871, China
[4] Institute de Radioastronomie Millimetrique, St. Martin d'Heres F-38406, France
[5] California Institute of Technology, 1200 East California Boulevard, Pasadena, CA 91125, USA
[6] European Southern Observatory, Alonso de Córdova 3107, Vitacura, Casilla 19001, Santiago 19, Chile
[7] Max-Planck-Institute for Astronomy, Königsstuhl 17, 69117 Heidelberg, Germany
[8] Argelander Institut für Astronomie, University of Bonn, Auf dem Hügel 71, 53121 Bonn, Germany
[9] Max-Planck-Institut für Radioastronomie, Auf dem Hügel 71, 53121 Bonn, Germany
[10] Institut d'Astrophysique de Paris, CNRS and Universite Pierre et Marie Curie, Paris, France
[11] Steward Observatory, The University of Arizona, Tucson, AZ 85721, USA
Received 2009 December 15; accepted 2010 February 5; published 2010 April 14

ABSTRACT

We report our new observations of redshifted carbon monoxide emission from six $z \sim 6$ quasars, using the IRAM Plateau de Bure Interferometer. CO (6–5) or (5–4) line emission was detected in all six sources. Together with two other previous CO detections, these observations provide unique constraints on the molecular gas emission properties in these quasar systems close to the end of the cosmic re-ionization. Complementary results are also presented for low-J CO lines observed at the Green Bank Telescope and the Very Large Array, and dust continuum from five of these sources with the SHARC-II bolometer camera at the Caltech Submillimeter Observatory. We then present a study of the molecular gas properties in our combined sample of eight CO-detected quasars at $z \sim 6$. The detections of high-order CO line emission in these objects indicates the presence of highly excited molecular gas, with estimated masses on the order of $10^{10}\ M_{\odot}$ within the quasar host galaxies. No significant difference is found in the gas mass and CO line width distributions between our $z \sim 6$ quasars and samples of CO-detected $1.4 \leqslant z \leqslant 5$ quasars and submillimeter galaxies. Most of the CO-detected quasars at $z \sim 6$ follow the far-infrared–CO luminosity relationship defined by actively star-forming galaxies at low and high redshifts. This suggests that ongoing star formation in their hosts contributes significantly to the dust heating at FIR wavelengths. The result is consistent with the picture of galaxy formation co-eval with supermassive black hole (SMBH) accretion in the earliest quasar–host systems. We investigate the black hole–bulge relationships of our quasar sample, using the CO dynamics as a tracer for the dynamical mass of the quasar host. The median estimated black hole–bulge mass ratio is about 15 times higher than the present-day value of ∼0.0014. This places important constraints on the formation and evolution of the most massive SMBH-spheroidal host systems at the highest redshift.

Key words: galaxies: active – galaxies: high-redshift – galaxies: starburst – molecular data – radio lines: galaxies

Online-only material: color figures

1. INTRODUCTION

Optically bright and massive quasar systems have been discovered at $z \sim 6$ through large optical surveys (e.g., Fan et al. 2006b; Willott et al. 2007, 2009a, 2009b; Cool et al. 2006; Jiang et al. 2008). The Gunn–Peterson absorption seen in their rest-frame UV spectra indicates that they exist close to the epoch of the cosmic re-ionization, and thus, are among the first generation of the most luminous objects in the universe (Fan et al. 2006a, 2006c). About 30% of the $z \sim 6$ quasars have been detected in dust continuum emission at 250 GHz, indicating large far-infrared (FIR) luminosities ($3 \times 10^{12}\ L_{\odot}$–$10 \times 10^{12}\ L_{\odot}$; Wang et al. 2008b) arising from dust with temperatures of 30–60 K (e.g., Benford et al. 1999; Petric et al. 2003; Bertoldi et al. 2003a; Beelen et al. 2006; Wang et al. 2007, 2008b). Studies of these objects' optical-to-radio spectral energy distributions (SEDs) and luminosity correlations argue for dust heating by star formation in the host galaxies (Bertoldi et al. 2003a; Beelen et al. 2006; Carilli et al. 2004; Riechers et al. 2007; Wang et al. 2008b). High resolution imaging of the dust continuum and [C II] λ 158 μm line emission in the brightest $z \sim 6$ millimeter source, the $z = 6.42$ quasar SDSS J114816.64+525150.3 (hereafter J1148+5251), suggest a high star formation surface density in the quasar host of $\sim$1000 $M_{\odot}\ \mathrm{yr}^{-1}\ \mathrm{kpc}^{-2}$ (Walter et al. 2009). It is likely that we are witnessing an early galaxy evolutionary stage in these FIR luminous quasar systems at $z \sim 6$, in which a massive starburst is ongoing coevally with a luminous central active galactic nuclei (AGNs). These objects therefore may also provide crucial insight into our understanding of the origin of the correlation between bulge mass/luminosity/stellar velocity dispersion and supermassive black hole (SMBH) mass in nearby galaxies (Tremaine et al. 2002; Marconi & Hunt 2003; Hopkins et al. 2007a), which suggests that the formation of the SMBH and its spheroidal host are tightly coupled (Kauffmann & Haehnelt 2000; Hopkins et al. 2007b).

Molecular CO line emission has been widely detected and studied in similar FIR luminous quasar systems at $z > 1$–5 (e.g., Brown & Vanden Bout 1992; Omont et al. 1996b; Carilli et al. 2002; Cox et al. 2002; Solomon & Vanden Bout 2005, hereafter SV05; Riechers et al. 2006; Maiolino et al. 2007; Coppin et al. 2008a). These CO detected quasars show an FIR-to-CO luminosity correlation similar to local starburst spiral

[12] Hubble Fellow.

galaxies, Ultra Luminous Infra Red Galaxies (ULIRGs), and high-z submillimeter galaxies (SMGs; SV05; Greve et al. 2005; Riechers et al. 2006). The derived molecular gas masses are on the order of $\sim 10^{10}\,M_{\odot}$, which are also comparable to the typical values found in SMGs (Greve et al. 2005; Carilli & Wang 2006; Coppin et al. 2008a) and the $z \sim 1.5$ massive star-forming disk galaxies (Daddi et al. 2008). The molecular gas can provide the requisite fuel for massive star formation which is suggested by the FIR emission redshifted to submillimeter and millimeter wavelengths (Benford et al. 1999; Omont et al. 1996a, 2003; Priddey et al. 2003; Robson et al. 2004; Beelen et al. 2006; Wang et al. 2008a).

The CO line emission detected in FIR luminous quasars provides estimates of the dynamical properties of the spheroidal bulges (i.e., bulge mass and velocity dispersion). Shields et al. (2006) investigated the relation between black hole mass ($M_{\rm BH}$) and bulge velocity dispersion (σ) in high-z quasar systems using the observed CO line widths. They found that the massive quasars ($M_{\rm BH} > 10^9$–$10^{10}\,M_{\odot}$) at $z > 3$ appear to have much narrower σ values compared to what is expected from the local $M_{\rm BH}$–σ relationship (e.g., Tremaine et al. 2002). Moreover, Coppin et al. (2008a) found that the average black hole–bulge mass ratios for CO and FIR luminous quasar samples at $z \sim 2$ are likely to be an order of magnitude higher than the local value ($M_{\rm BH}/M_{\rm bulge} \sim 0.0014$; Marconi & Hunt 2003). Less evolved stellar bulges were also indicated by high resolution imaging of the CO emission in two $z > 4$ quasars (Riechers et al. 2008a, 2008b). These results argue for the scenario that the formation of the SMBHs occurs prior to that of the stellar bulge, which is also suggested by the near-IR imaging of high-z quasar host galaxies (Peng et al. 2006a, 2006b).

CO line emission was previously searched in four $z \sim 6$ quasars, and detected in two of these (Walter et al. 2003; Bertoldi et al. 2003b; Carilli et al. 2007; Maiolino et al. 2007). The two CO-detected quasars, J1148+5251 and J0927+2001, are the brightest millimeter sources among a sample of 33 $z \sim 6$ quasars that have published millimeter dust continuum observations (Petric et al. 2003; Bertoldi et al. 2003a; Wang et al. 2007, 2008a). The detected CO transitions indicate highly excited molecular gas in the quasar host galaxies (line flux density SEDs peaking at $J = 6$ or higher; Carilli et al. 2007; Riechers et al. 2009) and the implied molecular gas masses are all $\sim 2 \times 10^{10}\,M_{\odot}$. High-resolution Very Large Array (VLA) imaging has resolved the CO emission in J1148+5251 to kpc scale, suggesting a dynamical mass of $M_{\rm dyn} \sin^2 i \sim 4.5 \times 10^{10}\,M_{\odot}$ within a radius of 2.5 kpc, where i is the inclination angle (Walter et al. 2004; Riechers et al. 2009) of the molecular disk. This provides the first direct constraint on the mass of the quasar host galaxy at the highest redshift, which suggests a high black hole–bulge mass ratio similar to that found with the $z \sim 2$ and $z > 4$ quasars.

In this work, we extend the CO observations to all $z \sim 6$ quasars with known 250 GHz continuum flux densities of $S_{250\,\rm GHz} \geqslant 1.8$ mJy (Wang et al. 2007, 2008b). We aim to study their general molecular gas properties and investigate possible constraints on the SMBH–host evolution with these earliest quasars. We describe the sample selection and observations in Section 2, and present the results in Section 3. The CO emission and gas properties of these $z \sim 6$ quasars are analyzed in Section 4. Based on our results, we present a brief discussion on the constraints of the black hole–bulge evolution in Section 5, and summarize the main conclusions in Section 6. A ΛCDM cosmology with $H_0 = 71\,{\rm km\,s^{-1}\,Mpc^{-1}}$, $\Omega_{\rm M} = 0.27$, and $\Omega_{\Lambda} = 0.73$ is adopted throughout this paper (Spergel et al. 2007).

2. SAMPLE AND OBSERVATIONS

2.1. Sample

There are 33 quasars at $z \sim 6$ that have published observations of dust continuum at 250 GHz that were made with the Max-Planck Millimeter Bolometer Array (MAMBO; Kreysa et al. 1998) on the IRAM 30 m telescope, and 10 of these have been detected (Bertoldi et al. 2003a; Petric et al. 2003; Willott et al. 2007; Wang et al. 2007, 2008b). The two brightest MAMBO detections (i.e., $S_{250\,\rm GHz} \sim 5$ mJy, $L_{\rm FIR} \sim 10^{13}\,L_{\odot}$), J1148+5251 and J0927+2001, have all been detected in strong molecular CO line emission (J1148+5251: CO (3–2), Walter et al. 2003; CO (7–6) and (6–5), Bertoldi et al. 2003b; J0927+2001: CO (6–5) and (5–4), Carilli et al. 2007). In this work, we present new observations of CO (6–5) and/or (5–4) line emission in another six $z \sim 6$ quasars (J0840+5624, J1044−0125, J1048+4637, J1335+3533, J1425+3254, J2054−0005) using the Plateau de Bure Interferometer (PdBI). They all have 250 GHz flux density of $S_{250\,\rm GHz} \geqslant 1.8$ mJy and corresponding FIR luminosities of $L_{\rm FIR} > 5 \times 10^{12}\,L_{\odot}$ (using the estimation given in Wang et al. 2008a, 2008b). We also report our observations of the CO (2–1) line in J0840+5624 and J0927+2001 with the Green Bank Telescope (GBT), CO (3–2) in J1048+4637 with the VLA, and 350 μm dust continuum in J0840+5624, J0927+2001, J1044−0125, J1335+3533, and J1425+3254 with the SHARC-II bolometer camera at the Caltech Submillimeter Observatory (CSO).

We list the basic information of all the eight FIR luminous $z \sim 6$ quasars in Table 1, including their redshifts from the discovery papers (Fan et al. 2000, 2003, 2006b; Jiang et al. 2008; Cool et al. 2006), optical magnitudes, continuum flux densities at 250 GHz and 1.4 GHz (Bertoldi et al. 2003a; Carilli et al. 2004; Wang et al. 2007, 2008b), as well as available measurements of the black hole masses and AGN bolometric luminosities (Jiang et al. 2006). These objects are mainly optically selected with rest-frame 1450 Å (m_{1450}) absolute magnitude of $-27.8 < M_{1450} < -26.0$, indicating AGN bolometric luminosity of $L_{\rm bol} > 10^{13}\,L_{\odot}$ (Jiang et al. 2006), which are among the brightest objects in the quasar population. The black hole masses of J1148+5251 and J1044−0125 have been determined from the measurements of the AGN UV broad line emission (Willott et al. 2003; Jiang et al. 2006) which are a few $10^9\,M_{\odot}$, indicating Eddington ratios of 0.5–1.0 (Jiang et al. 2006).

2.2. Molecular CO Observations

The observations of the CO (6–5) and (5–4) lines were carried out with the new generation 3 mm receiver on the PdBI, which provides a bandwidth of 1 GHz in dual polarization. The sources were observed between 2007 and 2009, in the compact D configuration (FWHM resolution $\sim 5''$). We generally used two frequency setups for the first two tracks on each target to cover a continuous bandwidth of 1.8 GHz, to account for the possible uncertainties between the optical and systemic (CO) redshifts. In the case of marginal detections, we added one more track with both polarization bands centered at the likely line frequency to confirm the line at $>3\sigma$ significance. The original frequency resolution is 2.5 MHz which was subsequently binned to 23 MHz ($\sim 70\,{\rm km\,s^{-1}}$). Phase calibration was performed every 20 minutes with observations of 0954+658, 1055+018, 1150+497, 1308+326, and 2134+004. We observed MWC 349

Table 1
Optical and Millimeter Measurements of the Sample

Name	z	m_{1450}	M_{1450}	$S_{250\,\mathrm{GHz}}$ (mJy)	$S_{1.4\,\mathrm{GHz}}$ (μJy)	Reference	L_{bol} ($10^{13}\,L_{\odot}$)	M_{BH} ($10^{9}\,M_{\odot}$)
(1)	(2)	(3)	(4)	(5)	(6)	(7)	(8)	(9)
J084035.09+562419.9	5.85	20.04	−26.66	3.20 ± 0.64	12 ± 9	[1, 2]	5.9	...
J092721.82+200123.7	5.79	19.87	−26.78	4.98 ± 0.75	50 ± 11	[1, 2, 3]	...	...
J104433.04−012502.2	5.80	19.21	−27.47	1.82 ± 0.43	−15 ± 24	[3, 4, 5]	11.8	6.4
J104845.05+463718.3	6.23	19.25	−27.55	3.00 ± 0.40	7 ± 13	[6, 7, 8]	9.8	...
J114816.64+525150.3	6.43	19.03	−27.82	5.00 ± 0.60	55 ± 12	[6, 7, 8]	19.3	5.6
J133550.81+353315.8	5.93	19.89	−26.82	2.34 ± 0.50	35 ± 10	[1, 2]	...	...
J142516.30+325409.0	5.85	20.62[a]	−26.09	2.27 ± 0.51	20 ± 20	[3, 9]	...	...
J205406.42−000514.8	6.06	20.60	−26.15	2.38 ± 0.53	17 ± 23	[3, 10]	...	...

Notes. We list the SDSS name in Column 1: the redshifts, AB magnitudes at rest frame 1450 Å from the discovery paper in Columns 2–4, 3. The 250 GHz and 1.4 GHz continuum measurements from the literatures are summarized and listed in Columns 5 and 6. Column 7 gives the references for the optical, millimeter, and radio data, with (1) Fan et al. 2006b; (2) Wang et al. 2007; (3) Wang et al. 2008b; (4) Fan et al. 2000; (5) Petric et al. 2003; (6) Fan et al. 2003; (7) Bertoldi et al. 2003a; (8) Carilli et al. 2004; (9) Cool et al. 2006; (10) Jiang et al. 2008. The last two columns list the available measurements of AGN bolometric luminosities and black masses from Jiang et al. (2006).

[a] Derived with the absolute AB magnitude at rest frame 1450 Å from Cool et al. (2006).

as the flux calibrator. The typical rms after 8 hr of observing time is about 0.5 mJy beam^{-1} per 70 km s^{-1} wide bin. The data were reduced with the IRAM GILDAS software package (Guilloteau & Lucas 2000).

We also conducted observations of CO (2–1) line emission in two of the CO-detected $z \sim 6$ quasars, J0840+5624 and J0927+2001, during the winter months of 2007–2008, using the Ka-band receiver on the 100 m GBT. The observations employed the subreflector nodding mode with half-cycle times between 9.0 and 22.5 s. The tunings were based on the CO (6–5)/(5–4) redshifts (Bertoldi et al. 2003b; Carilli et al. 2007). We set up the spectrometer in low resolution mode with two single-polarization 800 MHz windows centered at offsets of −100 MHz and +100 MHz from the observed line frequency. Thus, the two polarizations cover the redshifted CO (2–1) line with a bandwidth of 600 MHz simultaneously.

Flux calibration was performed using 3C147, and pointing was checked regularly on known radio sources. Data were analyzed using the data reduction routines in the GBTIDL software package. The uncertainties of the flux calibration are typically 10%–20%. We have spent 17.7 hr of observing time (including overhead due to subreflector movement) on J0840+5624, leading to an rms noise of about 0.13 mJy per 50 km s^{-1} wide channel, measured from the line-free channels. However, there is a small-scale baseline structure close to the observed line frequency, which cannot be removed in the calibration, and thus, precluded detection of weak line emission with peak flux density of a few hundred μJy (see Wagg et al. 2008). We also spent 10.7 hr on J0927+2001, and the CO (2–1) line is not detected with a 1σ rms sensitivity of 0.15 mJy per 50 km s^{-1} channel.

Finally, we report a tentative VLA Q-band detection of CO (3–2) line emission from J1048+4637. These observations were conducted in 2004 in BC, C, and CD configurations. The source was observed in continuum mode, i.e., two polarizations, two intermediate frequency bands "IFs," and 50 MHz bandwidth (∼310 km s^{-1} in velocity) per IF for each frequency setup. We searched the CO (3–2) line emission in the frequency range from 47.715 GHz to 48.165 GHz (corresponding to 6.179–6.247 in redshift) by observing the source repeatedly with different frequency setups.

We reduced the data and made images using the standard VLA wide field data reduction software AIPS and the source is detected in the 50 MHz channel centered at 47.865 GHz ($z = 6.224$, $\Delta z = 0.008$) at $\gtrsim 4\sigma$ with a 1σ rms of 70 μJy beam^{-1}. The spatial resolution on the final map is 0.″5 (FWHM). The 1σ rms values for the other channels are much higher, i.e., from 120 to 200 μJy beam^{-1} (due to less observing time) and no signal is detected at the quasar position. We excluded the data observed at 47.865 GHz and 47.815 GHz which are close to the CO (3–2) line frequency for $z = 6.2284$ (i.e., the redshift determined with the PdBI CO (6–5) detection), and merged the data of all the other channels to constrain the source continuum at 48 GHz. The 1σ rms noise on the combined image is 65 μJy beam^{-1} and no continuum emission is detected.

2.3. SHARC-II 350 μm Dust Continuum Observations

We obtained new 350 μm observations of the dust continuum emission from five $z \sim 6$ quasars, using the SHARC-II bolometer camera on the CSO 10.4 m telescope. The SHARC-II camera is a 12 × 32 element array with a field of view of 2.′6 × 1.′0 and a beam size of 8.″5. The observations were conducted in 2008 February during excellent weather conditions on Mauna Kea (opacity at 225 GHz < 0.06). We adopted a scan pattern similar to our previous SHARC-II observations of $z \sim 6$ quasars, i.e., a Lissajous pattern with amplitudes of ±45″ and ±12″ in azimuth and elevation, respectively. This provides a uniform coverage of ∼65″ × 34″. Pointing, focus, and flux calibrations were done on Mars, Saturn, and a number of secondary calibrators (OH 231.8+4.2, CRL 618, IRC 10216, Arp 220, and 3C345). The final calibration uncertainties are within 20%.

The on-source integration time for each of the five objects is listed in Table 2. Data reduction was performed with the CRUSH data reduction package version 1.63 (Kovács 2006) and the rms noise values in the final maps are <5 mJy beam^{-1} for all targets. With these new observations, we confirm a previous 350 μm detection of J0927+2001 and marginally detect the dust continuum toward J0840+5624 (2.9σ). The measurements and upper limits for the other three sources are listed in the next section.

3. RESULTS

We have detected CO (6–5) or (5–4) line emission at $\geqslant 5\sigma$ in all six quasars observed with the PdBI. The CO emission is unresolved for all the six objects with the 5″ synthesized

Table 2
Measurements of the CO Emission

Name	Transition	z_{CO}	FWHM (km s^{-1})	$I\Delta v$ (Jy km s^{-1})	$t_{on,PdBI}$ (hr)	$s_{con,3\,mm}$ (mJy)	$s_{con,350\,\mu m}$ (mJy)	$t_{on,SHARC}$ (hr)
(1)	(2)	(3)	(4)	(5)	(6)	(7)	(8)	(9)
J0840+5624	5−4	5.8441 ± 0.0013	860 ± 190	0.60 ± 0.07	31.4	0.10 ± 0.05	9.3 ± 3.2	7.3
	6−5			0.72 ± 0.15	8.2	−0.01 ± 0.10		
	2−1	...	...	<0.1[a]	...	...		
J0927+2001	2−1	5.7722 ± 0.0006[b]	...	<0.1	...	...	11.7 ± 2.4	12.0
J1044−0125	6−5	5.7824 ± 0.0007	160 ± 60	0.21 ± 0.04	19.8	0.10 ± 0.05	<13.5	2.3
J1048+4637	6−5	6.2284 ± 0.0017	370 ± 130	0.27 ± 0.05	30.1	0.13 ± 0.03	<17.4[d]	...
	3−2	...	310[c]	0.09 ± 0.02	...	...		
J1048NE	6−5	6.2259 ± 0.0019	∼550	0.23 ± 0.05	30.1	...	...	...
			...	0.58 ± 0.13[e]				
J1335+3533	6−5	5.9012 ± 0.0019	310 ± 50	0.53 ± 0.07	16.7	0.05 ± 0.05	<13.2	3.5
J1425+3254	6−5	5.8918 ± 0.0018	690 ± 180	0.59 ± 0.11	16.1	0.09 ± 0.04	<7.8	4.7
J2054−0005	6−5	6.0379 ± 0.0022	360 ± 110	0.34 ± 0.07	16.6	0.10 ± 0.05	...	...

Notes. Column 1: source names; Column 2: CO transitions observed in this work; Columns 3–5: redshifts, line widths, and flux measured with the CO detection; Column 6: on-source time; Column 7: dust continuum measurements under the CO line spectrum observed with PdBI; Columns 8 and 9: dust continuum measurements and on-source integration time with SHARC-II at 350 μm.

[a] Upper limits derived with the channel-to-channel rms noise. One should be cautious with this value as there is a small-scale structure close to the line frequency which preclude detection of weak line emission with peak flux density of a few hundred μJy (Wagg et al. 2008).

[b] Carilli et al. (2007) measured with the CO (6–5) and (5–4) line emission.

[c] Line width calculated with the 50 MHz channel width.

[d] Wang et al. (2008a).

[e] Primary beam attenuation-corrected line flux for J1048NE (see Figure 1).

beam (∼29.2 kpc at $z \sim 6$), and only one source, J1048+4637, has a clear detection of the 3 mm continuum in the line-free channels. We fit the line spectra with a single Gaussian profile to determine the line widths (FWHM), host-galaxy redshifts, and corresponding uncertainties. The line spectra with the Gaussian-fit profiles are presented in the left panel of Figure 1. The line fluxes are obtained by integrating the data over the line emitting channels. The averaged-intensity maps are presented in the right panel of Figure 1. The CO emission peaks on the intensity maps show offsets of 0.″3–1.″8 from the optical quasar positions (see details for each sources below), which are all within the relative astrometric uncertainties of the observations. We summarize the line and continuum parameters for the PdBI detections in Table 2. The CO (3–2) detection in J1048+4637, CO (2–1) upper-limits, and the 350 μm dust continuum measurements are also listed in this table. We show the 350 μm dust continuum maps of J0840+5624 and J0927+2001 in Figure 2. The VLA Q-band 47.865 GHz image of the CO (3–2) line detection in J1048+4637 is shown in the left panel of Figure 3. An average image of the line-free channels is also presented (right panel), which constrains the continuum emission from this object at 48 GHz.

3.1. Notes for Individual Objects

J0840+5624. Both the CO (6–5) and (5–4) transitions were detected, peaking at $08^h40^m35^s.08$, +56°24′20.″5, 0.″6 from the optical quasar position. The integrated line flux densities are 0.60 ± 0.07 Jy km s^{-1} and 0.72 ± 0.15 Jy km s^{-1}, respectively. A single Gaussian line profile fitted to the combined spectrum of the two CO transitions yields a host galaxy redshift of 5.8441 ± 0.0013 and a FWHM line width of 860 ± 190 km s^{-1}. This is the largest CO line width that we have detected among the $z \sim 6$ quasars, and the line profile is double peaked. A fit with two Gaussian components to the combined spectrum gives peak velocity offsets of −300 km s^{-1} and 230 km s^{-1}, and FWHM line widths of ∼300 km s^{-1} and 410 km s^{-1} for the two components, respectively. Continuum is not detected in the line-free channels and the 3σ upper limits are 0.15 mJy at 85 GHz and 0.30 mJy at 101 GHz.

The GBT observation of the CO (2–1) transition gives an rms of about 0.13 mJy per 50 km s^{-1} channel. Assuming a velocity range similar to the CO (5–4) line, We estimated a 3σ line flux upper limit of about 0.1 Jy km s^{-1} for this object.[13] However, we emphasize that there are large uncertainties in this measurement due to a small-scale baseline structure close to the expected line frequency (Wagg et al. 2008).

The 350 μm dust continuum emission is marginally detected in this object at ∼2.9σ. The continuum source is unresolved and peaks at R.A. = $08^h40^m35^s.32$, decl. = 56d24′17.″5, which is 3.″1 away from the optical quasar (the left panel of Figure 2). The peak value is 9.3 ± 3.2 mJy beam^{-1} on the final map and we adopt this as the tentative 350 μm flux density. Further 350 μm observations with better sensitivity are necessary to confirm this tentative detection. On the SHARC-II map, there is also a 4σ peak (14.8 ± 3.7 mJy) at the position of R.A. = $08^h40^m34^s.35$, decl. = 56d24′45.″0 (i.e., northwest to the quasar, see the left panel of Figure 2). We checked our previous VLA 1.4 GHz continuum observation (observed in A array with a resolution of FWHM ∼ 1.″4; Wang et al. 2007) and there is a radio source with $S_{1.4\,GHz} = 44 \pm 9$ μJy close to this position, i.e., at R.A. = $08^h40^m34^s.25$, decl. = 56d24′44.″7. The offset is only 0.″9, well within the position uncertainty of the SHARC-II observation. There is no further identification information for this field source yet.

J1044−0125. We detected the CO (6–5) line in this source, peaking at the position of $10^h44^m33.02$, −01°25′02.″3, 0.″3 away from the optical quasar. The FWHM of the CO line fitted with a single Gaussian profile is 160 ± 60 km s^{-1}, which represents

[13] The 3σ upper limits on the CO (2–1) line emission are estimated as $3\,\sigma_{channel}(\Delta v_{channel}\,\Delta v_{line})^{1/2}$ (in Jy km s^{-1}), where Δv_{line} is the expected CO line width in km s^{-1}, $\Delta v_{channel}$ is the channel width in km s^{-1}, and $\sigma_{channel}$ is the corresponding rms noise value in Jy (Seaquist et al. 1995; Wagg et al. 2007). We adopt the full line width at zero intensity from the PdBI spectrum as Δv_{line} in the calculation.

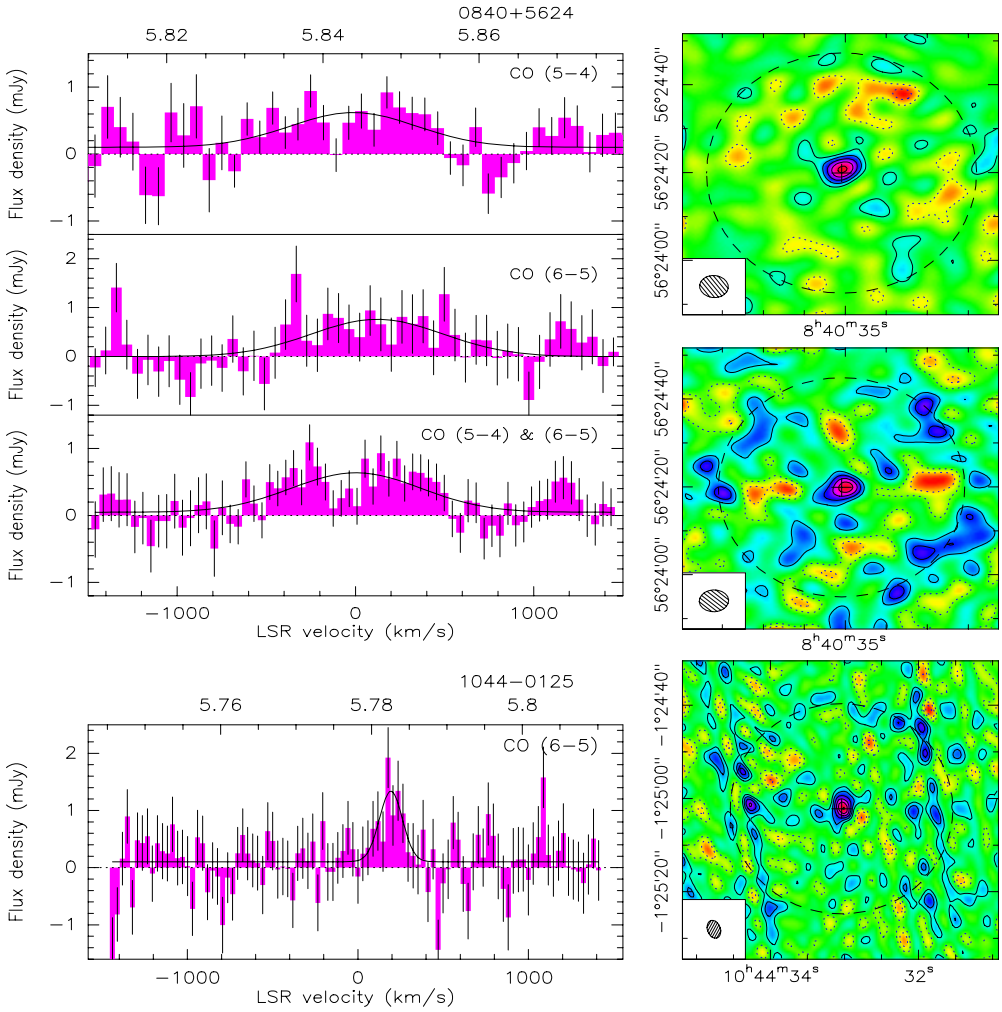

Figure 1. CO line spectra (left) and velocity-integrated images (right) of the six CO-detected quasars at $z \sim 6$. The top abscissae of the left plots give the redshift range of the spectra windows, and the zero velocities correspond to the redshifts of $z = 5.844$, 5.778, 6.200, 5.950, 5.877, and 6.070. The error bars in the spectra denote the 1σ rms noise in each channel, and the solid lines show Gaussian fits to the line emission. The third spectrum for J0840+5624 is a combined spectrum obtained by merging the data of the two detected CO transitions. In the spectrum of the NE source close to J1048+4637, the gray line indicates the primary beam attenuation-corrected line profile, assuming a line width of 370 km s^{-1}. The crosses on the images indicate the optical quasar position, and the dashed circles show the primary beam of the PdBI. On the map of J1044−0125, the spurious pattern to the east and west of the source is caused by the substantial sidelobes due to the strong signal from the central source.

(A color version of this figure is available in the online journal.)

the narrowest CO line width among all the CO-detected $z \sim 6$ quasars. The integrated line flux is 0.21 ± 0.04 Jy km s^{-1}. The 3σ upper limit on the continuum emission is 0.15 mJy at 102 GHz.

The 350 μm dust continuum emission has not been detected in our SHARC-II observations, and the 1σ rms is 4.5 mJy beam^{-1}. This yields a 3σ flux density upper limit of 13.5 mJy.

J1048+4637. We detected the CO (6–5) line emission in this source, peaking at $10^h48^m45.08$, 46°37′18.″7, 0.″5 away from the optical quasar position. The CO redshift is 6.2284 ± 0.0017, which is close to the value of 6.23 estimated from the Lyα+NV emission in the quasar rest-frame UV spectrum (Fan et al. 2003), but higher than the value of 6.19–6.20 measured from the Mg II λ2798 Å emission (Iwamuro et al. 2004; Maiolino et al. 2004b). The 3 mm dust continuum emission is detected along with the CO line emission. A simultaneous fit of the CO lines and the continuum gives a continuum flux density of 0.13 ± 0.03 mJy at 96 GHz. The integrated line flux is 0.27 ± 0.05 Jy km s^{-1}, and the FWHM line width from single Gaussian fit is 370 ± 130 km s^{-1}. We have also detected CO (6–5) line emission from a source ∼28″ away, to the northeast of the quasar (J1048NE). The CO spectrum yields a redshift of 6.2259 ± 0.0019 for this NE source, indicating the presence of a companion galaxy ∼160 kpc away from the optical quasar. The observed peak flux density is 0.53 ± 0.14 mJy, which gives an integrated flux of 0.23 ± 0.05 Jy km s^{-1}. Considering an attenuation factor of ∼0.4 for the primary beam (FWHM ∼ 52″) at the source position, we estimate the intrinsic line flux to be 0.58 ± 0.13 Jy km s^{-1} (see Figure 1).

The CO (3–2) line emission from this object was searched using the *Q*-band receiver on the VLA, and we detected the source at 0.30 ± 0.07 mJy in a 50 MHz wide channel centered at 47.865 GHz. The data averaged over the other channels present a 3σ upper limit of 0.195 mJy for the continuum emission at 48 GHz, indicating that the 0.3 mJy detection at 47.865 GHz are not due to nonthermal quasar continuum emission. An optically thin graybody model with a dust temperature of $T_{\rm dust} = 47$ K and an emissivity index of $\beta = 1.6$ (Beelen et al. 2006; Wang et al. 2008b) fitted to the continuum measurements at 250 GHz and 96 GHz suggests a continuum flux density of only 0.017 mJy

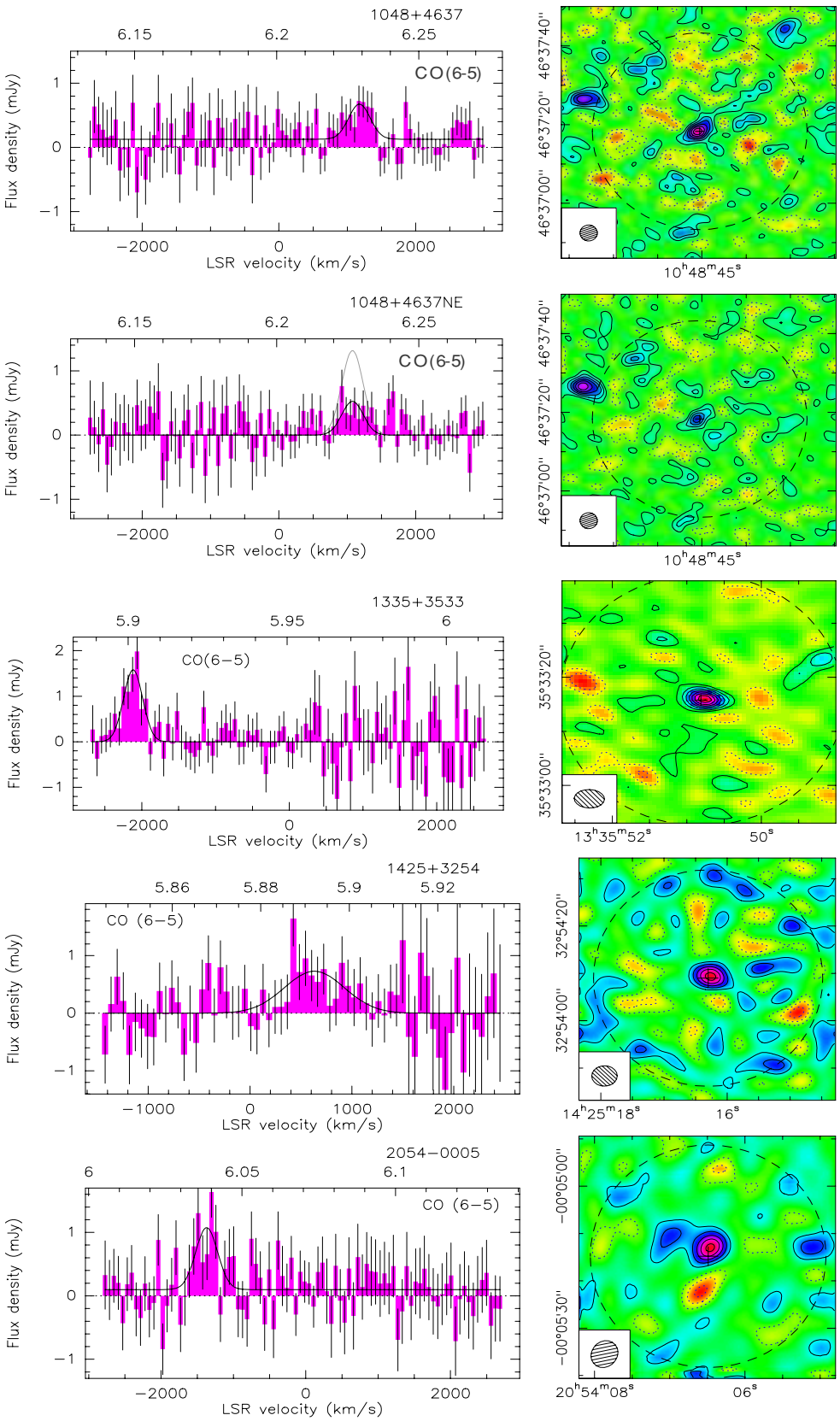

Figure 1. (Continued)

at the observed frequency of 47.865 GHz. Thus, the 0.30 mJy detection in this channel is likely to be from the CO (3–2) line emission. The source on the VLA image is marginally resolved by the 0.″5 × 0.″5 synthesized beam, and a fit to a two-dimensional-Gaussian component yields a source size of 0.″9 × 0.″4. The integrated line intensity detected in the channel is 0.09 ± 0.02 Jy km s^{-1}. According to the line profile and source redshift of $z = 6.2284 \pm 0.0017$ determined from the CO

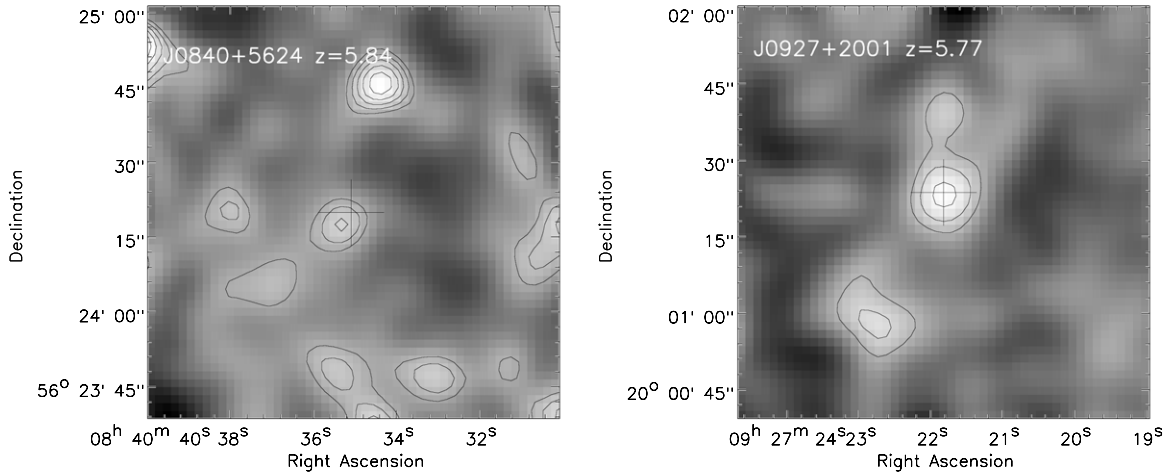

Figure 2. 350 μm maps of the SHARC-II marginally detected source J0840+5624 (left) and SHARC-II detected source J09227+2001 (right), smoothing to a beam size of FWHM = 12.″4. The contour levels are (2, 3, 4, 5, 6) × 2.2 mJy beam^{-1} for J0840+5624, and (2, 3, 4) × 2.7 mJy beam^{-1} for J0927+2001. The crosses denote the optical quasar positions.

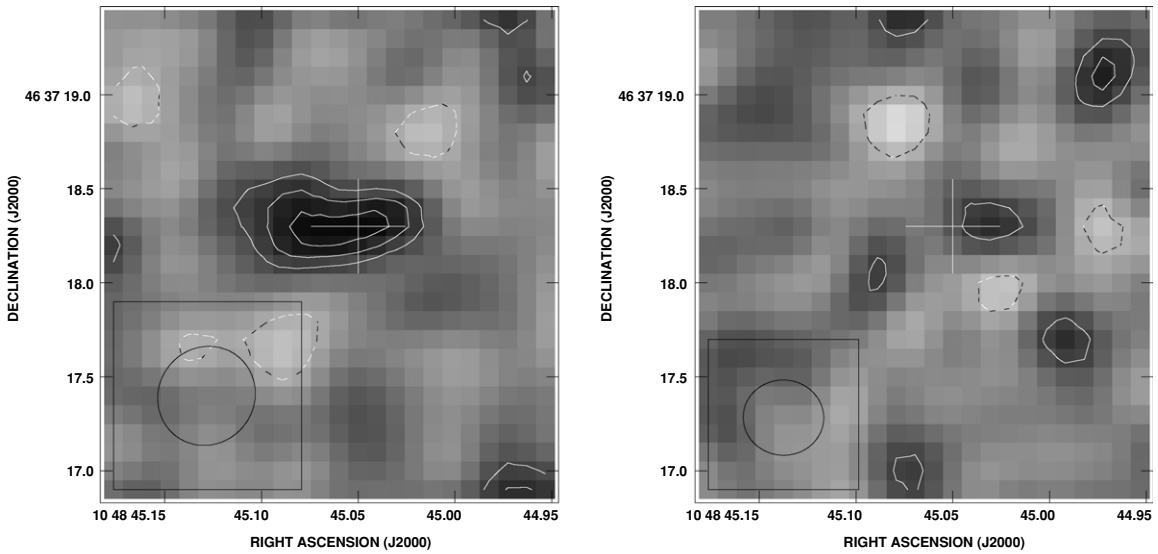

Figure 3. Left: the VLA *Q*-band image of the CO (3–2) line emission from J1048+4637 detected at 47.865 GHz (left) and a 48 GHz image averaged over the line-free channels (right). The 1σ rms values are 70 μJy beam^{-1} and 65 μJy beam^{-1} for the left and right images, respectively. The contour levels are (−2, 2, 3, 4) × 60 μJy beam^{-1} for both images. The ellipses indicate the beam sizes of 0.″5 × 0.″5 (FWHM) for the left plot and 0.″4 × 0.″4 for the right one, and the cross marks the optical quasar position.

(6–5) transition, the VLA observation is likely to be centered at the blue part of the CO (3–2) line emission and covers a bandwidth of 310 km s^{-1} in velocity. Thus, we adopt the measurement as a lower limit of the CO (3–2) line flux for this object.

J1335+3533. The CO (6–5) line was detected in this source, peaking at the position of $13^{\rm h}35^{\rm m}50\overset{\rm s}{.}75$, 35°33′15.″8, 0.″7 away from the optical quasar position. The CO FWHM fitted with a single Gaussian profile is 310 ± 50 km s^{-1}. The integrated line intensity is 0.53 ± 0.07 Jy km s^{-1}, and the 3σ upper limit on the continuum emission is 0.15 mJy at 100 GHz.

No 350 μm dust continuum is detected in our SHARC-II observations of this object. The 1σ rms on the final map is 4.4 mJy beam^{-1}, and the corresponding 3σ upper limit is 13.2 mJy for the 350 μm flux density.

J1425+3254. The CO (6–5) line was detected, peaking at the position of $14^{\rm h}25^{\rm m}16\overset{\rm s}{.}26$, 32°54′09.″3, 0.″6 away from the optical quasar. The CO FWHM fitted with a single Gaussian profile is 690 ± 180 km s^{-1}, and the line flux of 0.59 ± 0.11 Jy km s^{-1}. The 3σ upper limit for the continuum at 101 GHz is 0.12 mJy.

This source was not detected in our SHARC-II observations of the 350 μm dust continuum with a 1σ rms of 2.6 mJy beam^{-1}. This yields a 3σ upper limit of 7.8 mJy for the 350 μm flux density.

J2054−0005. The CO (6–5) line was detected in this source, peaking at the position of $20^{\rm h}54^{\rm m}06\overset{\rm s}{.}45$, −00°05′13.″1, 1.″8 away from the optical quasar. The CO line FWHM obtained from a fit to a single-Gaussian line profile is 360 ± 110 km s^{-1}. The derived integrated intensity is 0.34 ± 0.07 Jy km s^{-1}, and the 3σ upper limit on the continuum emission at 98 GHz is 0.15 mJy.

J0927+2001. We have observed the CO (2–1) line in this object for 10.7 hr with the GBT, and the final rms is 0.15 mJy per 50 km s^{-1} channel. We adopt a line width of ∼900 km s^{-1} (full width at zero intensity) based on the previous PdBI detections of the CO (6–5) and (5–4) transitions (Carilli et al. 2007), and derive a 3σ upper-limit to the integrated line intensity of ∼0.1 Jy km s^{-1}.

Table 3
Redshift Measurements

Name	z_{CO}	$z_{Ly\alpha}$	Reference	$z_{Mg\,II}$	Reference	$z_{C\,VI}$	Reference	$z_{U\,V}$[a]	Reference
(1)	(2)	(3)	(4)	(5)	(6)	(7)	(8)	(9)	(10)
J0840+5624	5.8441 ± 0.0013	5.85 ± 0.02	(1)			5.774	(2)		
J0927+2001	5.7722 ± 0.0006	5.79 ± 0.02	(1)						
J1044−0125	5.7824 ± 0.0007			5.78	(3)	5.745 ± 0.030	(4)	5.80 ± 0.02	(5)
								5.778 ± 0.005	(12)
J1048+4636	6.2284 ± 0.0017	6.23 ± 0.05	(6)	6.203	(7)				
				6.22	(8)				
				6.193	(9)				
J1148+5251	6.4192 ± 0.0009[b]	6.43 ± 0.05	(6)	6.41 ± 0.01	(10)			6.421	(2)
	6.4189 ± 0.0006[c]			6.40	(8)				
J1335+3533	5.9012 ± 0.0019	5.93 ± 0.04	(1)						
J1425+3254	5.8918 ± 0.0018	5.85 ± 0.02	(11)						
J2054−0005	6.0379 ± 0.0022	6.062 ± 0.004	(13)						

Notes.
[a] Redshift measured from other UV emission lines, such as the C III] λ1909 Å, O I+Si II λ1302 Å, and Si IV+O IV λ1400 Å.
[b] Redshift measured from the CO (7–6) line (Bertoldi et al. 2003b).
[c] Redshift measured from the CO (6–5) line (Bertoldi et al. 2003b).
References. (1) Fan et al. 2006b; (2) Ryan-Weber et al. 2009; (3) Freudling et al. 2003; (4) Goodrich et al. 2001; (5) Fan et al. 2000; (6) Fan et al. 2003; (7) Iwamuro et al. 2004; (8) Maiolino et al. 2004a; (9) Maiolino et al. 2004b; (10) Willott et al. 2003; (11) Cool et al. 2006; (12) Jiang et al. 2007; (13) Jiang et al. 2008.

The 350 μm dust continuum emission from this object was previously detected by our SHARC-II observations in 2007 (17.7 ± 5.7 mJy; Wang et al. 2008a). The new data we presented here confirm the detection with better sensitivity, i.e., a 350 μm flux density of 11.7 ± 2.4 mJy. This 350 μm dust continuum peak is quite consistent with the optical quasar position (offset of $< 1''$). We cannot confirm the $\sim 3\sigma$ peak $15''$ away from the quasar position reported in our previous work (Wang et al. 2008a).

3.2. CO Redshifts

We compare the redshifts determined from CO and UV emission lines in Table 3 for all CO detected $z \sim 6$ quasars, including the previous CO-detections in J1148+5251 and J0927+2001 (Bertoldi et al. 2003b, Carilli et al. 2007). The C IV λ1549 Å redshifts of J0840+5624 and J1044−0125 are blueshifted by about 3000 and 1600 km s^{-1} compared to the values determined from the CO lines, respectively. This is consistent with the fact that the C IV emission is typically blueshifted from the quasar systematic redshift by up to a few thousand km s^{-1} (Richards et al. 2002; Goodrich et al. 2001; Ryan-Weber et al. 2009). There is no systematic offset between the CO redshifts and those determined from other UV emission lines. In particular, the CO redshifts of J1044−0125 and J1148+5251 are in good agreement with the values derived from the C III] λ1909 Å and Si IV λ1400 Å broad emission lines with high-quality near-infrared spectroscopy (Jiang et al. 2007; Ryan-Weber et al. 2009). The largest offset between CO and Lyα redshifts is ∼0.04, which is reasonable since the Lyα redshifts are always poorly constrained (with uncertainties of 0.02–0.05).[14] Three objects have redshifts determined from the Mg II λ2798 Å line. The CO redshifts of J1044−0125 and J1148+5251 are consistent with the Mg II measurements within the uncertainties, while a large offset of ∼0.03 is seen in J1048+4637 between the CO redshift and the Mg II ones quoted in Iwamuro et al. (2004b) and Maiolino et al. (2004b).

[14] Note that the Lyα redshift uncertainty of 0.004 quoted in Jiang et al. (2008) is only an error from their spectral fitting.

4. ANALYSIS

Our PdBI observations have a 100% CO detection rate among the millimeter (FIR) luminous quasars in the early universe. Together with the previous CO detections in J1148+5251 and J0927+2001 (Bertoldi et al. 2003b; Walter et al. 2003, 2004; Carilli et al. 2007), all eight $z \sim 6$ quasars with published 250 GHz flux densities of $S_{250\,\mathrm{GHz}} \geqslant 1.8$ mJy (Bertoldi et al. 2003a; Wang et al. 2007, 2008b) have now been detected in CO (6–5) and/or (5–4) line emission. In this section, we present a study of the CO emission line properties in the earliest quasar host galaxies with this sample. We compare their molecular gas masses and CO line width distributions to that of the CO-observed quasars and SMGs at lower redshift. A list of 15 CO detected quasars at $1.4 \leqslant z \leqslant 4.7$ was summarized in SV05. Another quasar, SDSS J0338+0021, at $z = 5.0267$ was detected in CO (5–4) line emission by Maiolino et al. (2007). Additionally, Coppin et al. (2008a) presented six CO-detected quasars at $1.7 \leqslant z \leqslant 2.6$ (one of these is also in the SV05's sample). These give a sample of 21 CO-detected quasars with redshifts from 1.4 to 5. We also consider a sample of 14 CO-detected SMGs at $1.1 \leqslant z \leqslant 3.4$ from Greve et al. (2005) and Tacconi et al. (2006).

4.1. Molecular Gas Masses

The mass of the molecular gas in J1148+5251 is well determined from the CO (3–2) data (Walter et al. 2003, 2004; Riechers et al. 2009). The high-order CO transitions ($J \geqslant 5$) detected in SMGs and high-redshift quasars are usually not thermalized (e.g., Weiß et al. 2005a, 2007; Riechers et al. 2009). Thus, for the other seven CO-detected $z \sim 6$ quasars, we adopt the line ratios of $L'_{CO(6-5)}/L'_{CO(1-0)} \approx 0.78$ and $L'_{CO(5-4)}/L'_{CO(1-0)} \approx 0.88$ from the multi-CO transition large velocity gradient (LVG) modeling of J1148+5251 (Riechers et al. 2009) and use these numbers to calculate the CO (1–0) line luminosities ($L'_{CO(1-0)}$). We then estimate the molecular gas masses ($M_{gas} = M[H_2 + He]$) within the CO emitting region of the quasar host galaxies using $M_{gas} = \alpha L'_{CO(1-0)}$. An integrated CO intensity-to-gas mass conversion factor of

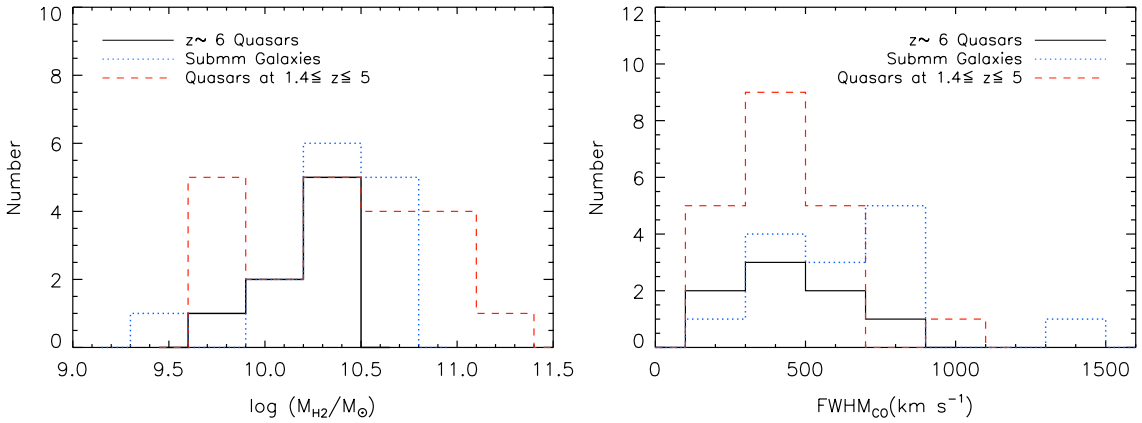

Figure 4. Molecular gas mass (left) and CO line width (right) distributions of the CO-detected $z \sim 6$ quasars, the SMGs, and $1.4 \leqslant z \leqslant 5$ quasars. (A color version of this figure is available in the online journal.)

Table 4
Derived Parameters

Name	$L'_{\rm CO}$ (10^{10} K km s^{-1} pc^2)	$L'_{\rm CO(1-0)}$ (10^{10} K km s^{-1} pc^2)	$L_{\rm FIR}$ ($10^{12}\,L_\odot$)	SFR ($M_\odot$ yr^{-1})	$M_{\rm dyn}\sin^2 i$ ($10^{10}\,M_\odot$)	$M_{\rm gas}$ ($10^{10}\,M_\odot$)
(1)	(2)	(3)	(4)	(5)	(6)	(7)
J0840+5624	2.8 ± 0.3[a]	3.2 ± 0.4	7.2 (5.7)	1460	24.2/4.2	2.5
J0927+2001	2.0 ± 0.3[a]	2.3 ± 0.4	8.5 (6.7)	1740	11.8	1.8
J1044−0125	0.7 ± 0.1[b]	0.8 ± 0.2	5.2 (2.0)	530	0.8	0.7
J1048+4637	1.0 ± 0.2[b]	1.2 ± 0.2	5.9 (2.5)	650	4.5	1.0
J1148+5251	3.0 ± 0.3[c]	3.0 ± 0.3	13.6 (9.2)	2380	4.6	2.4
J1335+3533	1.7 ± 0.2[b]	2.2 ± 0.3	5.5 (3.8)	970	3.1	1.8
J1425+3254	1.9 ± 0.4[b]	2.5 ± 0.5	5.4 (4.5)	1160	15.6	2.0
J2054−0005	1.2 ± 0.2[b]	1.5 ± 0.3	5.5 (4.6)	1180	4.2	1.2

Notes. Column 1: source name; Column 2: line luminosities of (a) the CO (5–4) transition (Carilli et al. 2007; this work), (b) the CO (6–5) transition (this work), and (c) the CO (3–2) transition (Walter et al. 2003; Riechers et al. 2009) in 10^{10} K km s^{-1} pc^2 (see, e.g., SV05 for the calculation), which are used to derive $L'_{\rm CO(1-0)}$ in the next column (See Section 4.1 for details); Column 3: the derived CO (1–0) luminosity; Column 4: FIR luminosity derived with the submillimeter and millimeter continuum data from the literature, and the values quoted in brackets are the AGN-corrected FIR luminosity (see Section 4.4 for details); Column 5: SFR derived with the AGN-corrected FIR luminosity; Column 6: dynamical masses derived with the observed CO line widths as was described in Section 5.2.1. The two values for J0840+5624 are derived with the single-Gaussian fitted FWHM of 860 km s^{-1} and the average peak offset of 270 km s^{-1}, respectively. We adopt the CO line widths of FWHM = 600 km s^{-1} for J0927+2001 from Carilli et al. (2007), and FWHM = 297 km s^{-1} from Walter et al. (2009) for J1148+5251. Column 7: molecular gas masses derived with $L'_{\rm CO(1-0)}$.

$\alpha = 0.8\,M_\odot\,(\mathrm{K\,km\,s^{-1}\,pc^2})^{-1}$, appropriate for ULIRGs, is adopted here (Solomon et al. 1997; Downes & Solomon 1998; SV05). The derived molecular gas masses are in the range, 0.7×10^{10}–$2.5 \times 10^{10}\,M_\odot$ (Table 4) with a median value of $1.8 \times 10^{10}\,M_\odot$.

We plot the molecular gas mass distribution of the $z \sim 6$ quasars, CO-observed SMGs, and $1.4 \leqslant z \leqslant 5$ quasars in the left panel of Figure 4. The range of gas masses of the $z \sim 6$ quasars (0.7×10^{10} to $2.5 \times 10^{10}\,M_\odot$) appears narrower but still comparable to the typical values found in the other two samples. We performed the standard Kolmogorov–Smirnov test between the $z \sim 6$ quasars and the other two samples. The probabilities that the data are drawn from the same parent population are 19% for the $z \sim 6$ and $1.4 \leqslant z \leqslant 5$ quasar samples, and 16% for the $z \sim 6$ quasar and SMG samples. This agrees with the results from previous studies that the high-z FIR and CO luminous quasars show molecular gas mass distribution similar to that of the SMGs (Carilli & Wang 2006; Coppin et al. 2008a).

4.2. CO Line Widths

The CO line widths (FWHM) of the $z \sim 6$ quasar sample are spread over a wide range, from 160 km s^{-1} to 860 km s^{-1}, with a median value[15] of 360 km s^{-1}. The broadest CO line detection (J0840+5624) appears to be double-peaked with peak-velocity offsets of ∼270 km s^{-1} (see Figure 1). Similar line profiles are widely observed in samples of SMGs (Greve et al. 2005; Weiß et al. 2005a; Tacconi et al. 2006), which may be due to either uncoalesced molecular gas components in a galaxy merger or simply reflect a large inclination angle of an extended gas disk relative to the sky plane.

In the right panel of Figure 4, we compare the CO line-width distribution of the $z \sim 6$ quasar sample to that of the CO-detected SMGs (Greve et al. 2005; Tacconi et al. 2006) and $1.7 \leqslant z \leqslant 5$ quasars (SV05; Coppin et al. 2008a). The Kolmogorov–Smirnov tests return probabilities of 13% for $z \sim 6$ quasars and SMGs, and 71% for $z \sim 6$ and $1.7 \leqslant z \leqslant 5$ quasars, i.e., there is no significant difference in the line-width distributions. This result confirms that the observed line-width distribution of high-z CO and FIR quasars is comparable to that of the SMGs as was found in Coppin et al. (2008a). The systemic difference reported in previous works (Greve et al. 2005; Carilli & Wang 2006) is likely to be due to selection effects and small sample size.

[15] The median value is the average of the two middle values if an even number of data points are presented in the sample.

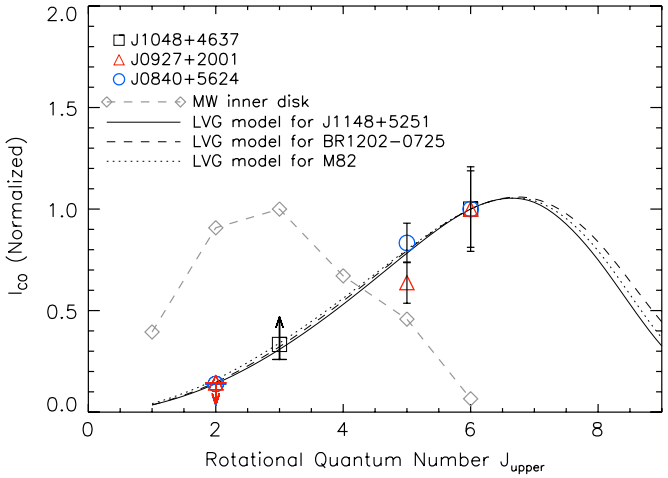

Figure 5. CO SEDs of J0840+5624 (blue circles), J0927+2001 (red triangles), and J1048+4637 (black squares). The arrow with black square represents the VLA detection of the CO (3–2) line emission from J1048+4637 in a 50 MHz channel, which provides a lower limit of the total line intensity due to the narrow bandwidth. The error bars show the 1σ uncertainties of the integrated line intensities. The solid line and dashed line show the LVG models of J1148+5251 with $T_{\rm kin} = 50$ K, $\rho_{\rm gas}(H_2) = 10^{4.2}$ cm^{-3} from Riechers et al. (2009) and BR 1202−0725 with $T_{\rm kin} = 60$ K, $\rho_{\rm gas}(H_2) = 10^{4.1}$ cm^{-3} from Riechers et al. (2006), respectively. The dotted line represents the LVG model of the high excitation component in the nearby starburst galaxy M82 with $T_{\rm kin} = 50$ K, $\rho_{\rm gas}(H_2) = 10^{4.2}$ cm^{-3} from Weiß et al. (2005b). We also plotted the CO excitation ladder of the Milky Way inner disk region for comparison (diamonds with light dashed line; Fixsen et al. 1999). The CO line intensities are normalized to the CO (3–2) line for the Milky Way and CO (6–5) for other sources and models.

(A color version of this figure is available in the online journal.)

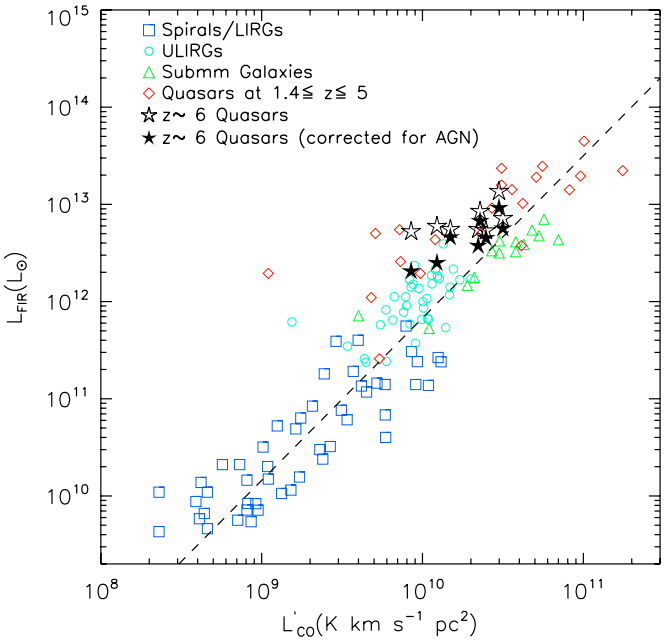

Figure 6. $L_{\rm FIR}$ vs. CO luminosity ($L'_{\rm CO}$). The data of samples at $z \leqslant 5$ are taken from Gao & Solomon (2004), Greve et al. (2005), Tacconi et al. (2006), Solomon et al. (1997), SV05, Riechers et al. (2006), Maiolino et al. (2007), and Coppin et al. (2008a). The dashed line represents the relationship $L_{\rm FIR} \propto L'^{1.67}_{\rm CO}$ fitted to the samples of local spirals, LIRGs, ULIRGs, and SMGs. The open stars represent the eight CO detected quasars at $z \sim 6$ with $L_{\rm FIR}$ estimated from (sub)mm observations, and the filled stars denote the values when contributions from AGNs are subtracted (see Section 4.4 for details).

(A color version of this figure is available in the online journal.)

4.3. Molecular CO Excitation

The detection of CO (6–5) line emission in all eight $z \sim 6$ quasars in our sample implies highly excited molecular gas in their host galaxies. Four of the CO-detected $z \sim 6$ quasars, J0840+5624, J0927+2001, J1048+4637, and J1148+5251, have observations of multiple CO line transitions (Bertoldi et al. 2003b; Carilli et al. 2007; this work). The CO "excitation ladder" of J1148+5251 has been studied by Bertoldi et al. (2003b) and Riechers et al. (2009), and the best LVG model fitted to the data suggests CO emission from a single gas component with kinetic temperature of $T_{\rm kin} = 50$ K and a molecular gas density of $\rho_{\rm gas}(H_2) = 10^{4.2}$ cm^{-3}. Similar CO excitation conditions are also found in the CO and FIR luminous quasar BR 1202−0725 at $z = 4.69$ (Carilli et al. 2002; Riechers et al. 2006) and some nearby starburst galaxies (e.g., the high excitation component in M82; Weiß et al. 2005b). In Figure 5, we plot the CO excitation ladders of J0840+5624, J0927+2001, and J1048+4637, together with the LVG models of J1148+5251, BR 1202−0725, and the high excitation component in M82. The line intensity ratios of $I_{\rm CO(5-4)}/I_{\rm CO(6-5)}$ for J0840+5624 and lower limit of $I_{\rm CO(3-2)}/I_{\rm CO(6-5)}$ for J1048+4637 are consistent with the model values. J0927+2001 shows a lower value of $I_{\rm CO(5-4)}/I_{\rm CO(6-5)}$ compared to the model, which, however, is still marginally consistent given the large uncertainties in the measurements of both transitions. These results suggest that such a warm, highly excited, single component gas model is a reasonable description of the molecular gas in all of these quasar host galaxies. Further observations of additional CO transitions in the CO-detected $z \sim 6$ quasars will address how the CO excitation properties vary among these objects.

4.4. FIR-to-CO Luminosity Relationship

The FIR luminosities, $L_{\rm FIR}$, of the eight CO-detected quasars at $z \sim 6$ are derived using the submillimeter and millimeter continuum measurements from the literature and the CO observations in this work (Bertoldi et al. 2003a; Beelen et al. 2006; Wang et al. 2007, 2008a, 2008b; Carilli et al. 2007), as listed in Table 4. A dust emissivity index of $\beta = 1.6$ (Beelen et al. 2006) is adopted in these calculations. J1148+5251 has a fitted dust temperature, $T_{\rm dust}$, of 56 K (Beelen et al. 2006) and J0927+2001 has $T_{\rm dust} = 46$ K, from fits to the submillimeter and millimeter measurements (this work; Wang et al. 2007, 2008a; Carilli et al. 2007; Riechers et al. 2009). We adopt the average dust temperature of 47 K found in high-z quasar host galaxies (Beelen et al. 2006) for the other six objects (see Wang et al. 2008b).

We plot $L_{\rm FIR}$ versus $L'_{\rm CO(1-0)}$ for the eight $z \sim 6$ quasars in Figure 6 and compare them with the local spiral, infrared luminous galaxies (LIRGs; Gao & Solomon 2004), ULIRGs (Solomon et al. 1997), the $1.4 \leqslant z \leqslant 5$ quasars, and SMG samples discussed above. For the high-z samples, $L_{\rm FIR}$ is recalculated using (sub)mm measurements from the literature (Smail et al. 2002; Kovács et al. 2006; Chapman et al. 2005; Omont et al. 2003; Benford et al. 1999; Beelen et al. 2006), using the β value mentioned above. We assume $T_{\rm dust} = 47$ K for the objects with less than three (sub)mm measurements in the quasar sample (Beelen et al. 2006), while $T_{\rm dust} = 35$ K is used for the SMGs, which is typical for the $T_{\rm dust}$ values found in previous (sub)mm studies (Kovács et al. 2006; Coppin et al. 2008b). The $z \sim 6$ quasars fall along the trend defined by all the other samples systems within the scatter (see the open stars in Figure 6).

A fit to the samples of local spirals, LIRGs, ULIRGs, and SMGs using the ordinary least squares bisector method (Isobe et al. 1990) yields a relationship of $\log L_{\rm FIR} = 1.67 \times \log L'_{\rm CO(1-0)} - 4.87$ for these typical star-forming systems, which is consistent with the result of $\log L_{\rm FIR} = 1.7 \times \log L'_{\rm CO(1-0)} - 5$ quoted in SV05 with similar samples. We also note that the $z \sim 6$ quasars all lie above this relationship. There are a number of undetermined parameters for individual objects, e.g., unknown AGN contributions to the FIR emission, different dust temperatures, and CO line ratios, which may account for the offsets and scatters. Further observations at infrared, submillimeter, and millimeter wavelengths will be important to directly probe the infrared SEDs and better constrain the dust temperatures and AGN contributions for these objects. For a rough estimation, we derive the AGN contributions to the FIR emission for our sample with the quasar rest frame 1450 Å continuum (Table 1) and a FIR-to-1450 Å luminosity ratio of $L_{\rm FIR}/\nu L_{\nu,1450\,\text{Å}} = 0.14$ from the local radio quiet quasar template (Elvis et al. 1994). The estimated AGN-dominated FIR emission is 0.9–4.4 $\times 10^{12}\,L_\odot$ for the eight sources, which account for about 30% of the FIR luminosities we calculated above with the (sub)mm observations on the average. We subtract these from the original $L_{\rm FIR}$ values (Table 1) and the corrected data points (see the filled stars in Figure 6) show a better agreement with the FIR-to-CO luminosity relationship for the star-forming system.

5. DISCUSSION

5.1. Star-forming Activity in the Millimeter and CO-detected Quasars at $z \sim 6$

CO emission has been detected toward the eight $z \sim 6$ quasars with published 250 GHz dust continuum flux densities of $S_{250\,\rm GHz} \geqslant 1.8$ mJy, indicating $\gtrsim 10^{10}\,M_\odot$ of molecular gas in the host galaxies of the FIR luminous quasars at the earliest epoch. The derived FIR and CO (1–0) luminosities follow the $L_{\rm FIR}$–$L'_{\rm CO}$ relationship defined by star-forming systems at low and high redshifts, suggesting a star formation origin of a dominant fraction of the FIR emission in most of these objects, i.e., the excess FIR dust emission is powered by star-forming activity in the circumnuclear region, not the central AGNs (Bertoldi et al. 2003a; Wang et al. 2008b; Walter et al. 2009). This is consistent with the idea of co-eval star formation with SMBH accretion in the massive $z \sim 6$ quasar systems which are bright at both UV-optical and FIR wavelengths (e.g., Bertoldi et al. 2003a, 2003b; Wang et al. 2007, 2008a, 2008b; Walter et al. 2003, 2004, 2009).

The measurements of (sub)mm dust continuum and molecular CO line emission from the quasar host galaxies provide the first constraint on the star-forming activities in these objects. Using the AGN contribution-removed FIR luminosities derived in the previous section (Table 1), we estimate the star formation rates (SFRs)[16] for the eight $z \sim 6$ quasars to be ~530–2380 $M_\odot\,{\rm yr}^{-1}$ (Kennicutt 1998). The ratios between SFR and $M_{\rm gas}$ (i.e., SFR per solar mass of molecular gas) provide a measure of the star formation efficiency, which are about $5 \times 10^{-8}\,{\rm yr}^{-1}$–$1 \times 10^{-7}\,{\rm yr}^{-1}$. This is comparable to that of the SMGs, $1.4 \leqslant z \leqslant 5$ CO-detected quasars, and local ULIRGs (SV05), and systematically higher than that of the local normal spiral disks (Kennicutt 1998), and high-z star-forming disk galaxies (e.g., the $z \sim 1.5$ BzK galaxies; Daddi et al. 2008, 2010), suggesting a high star formation efficiency in the host galaxies of these FIR and CO luminous $z \sim 6$ quasars similar to that of the extreme starburst systems (Tacconi et al. 2006; Walter et al. 2009). The inverse gives the gas depletion timescales of $\tau_{\rm dep} = M_{\rm gas}/{\rm SFR} \sim (1\text{–}2) \times 10^7$ yr.

[16] Calculated with ${\rm SFR} \sim 1.7 \times 10^{-10} L_{\rm IR}$ ($M_\odot\,{\rm yr}^{-1}$), where $L_{\rm IR}$ is the infrared luminosity (8–1000 μm) in units of $L_\odot$. We assume $L_{\rm IR}$ is ~1.5 $L_{\rm FIR}$ for 40–60 K warm dust emission.

5.2. Black Hole–Bulge Evolution

Massive bursts of star formation are likely to be on-going in these FIR and CO bright quasars at $z \sim 6$. In this section, we investigate the possible constraints of the black hole–bulge masses and velocity dispersion relationships in these $z \sim 6$ quasar systems using the available CO measurements. The available SMBH masses and AGN bolometric luminosities ($L_{\rm bol}$) from the literature are listed in Table 1. For other objects, we adopt the $L_{\rm bol}$ values estimated in Wang et al. (2008b) from M_{1450}, corrected to the CO redshifts, and estimated the black hole masses assuming $L_{\rm bol}/L_{\rm EDD} = 1$ and $M_{\rm BH} = L_{\rm bol}({\rm erg\,s^{-1}})/1.26 \times 10^{38}\,M_\odot$. The estimated $M_{\rm BH}$ values are all of the order of $10^9\,M_\odot$

5.2.1. $M_{\rm BH}$–$M_{\rm bulge}$ Relationship

The dynamical masses ($M_{\rm dyn}$) of the eight $z \sim 6$ quasars can be expressed as $M_{\rm dyn} \approx 2.3 \times 10^5 {v_{\rm cir}}^2 R$ (e.g., Neri et al. 2003; Walter et al. 2004; SV05; Narayanan et al. 2008), where R is the disk radius in kpc and $v_{\rm cir}$ is the maximum circular velocity of the gas disk in km s^{-1}. High-resolution CO observations of J1148+5251 give a gas disk radius of ~2.5 kpc and a dynamical mass of $4.5 \times 10^{10}\,M_\odot$. In the absence of spatially resolved measurement for our sample quasars, we here assume a disk radius of 2.5 kpc also for the other seven objects and estimate $v_{\rm cir}$ using 1/2 of the full width at 20% maximum (Ho 2007a, 2007b), which corresponds to about 3/4 of the CO FWHM for a single-Gaussian profile i.e., $v_{\rm cir} = 3{\rm FWHM}/4 \sin i$, where i is the inclination angle of the molecular gas disk. We leave $\sin i$ as an unknown factor in these calculations. The derived $M_{\rm dyn} \sin^2 i$ are from 8.4×10^9 to $2.4 \times 10^{11}\,M_\odot$ (Table 4). For 0840+5624, if we adopt the average peak-velocity offset of 270 km s^{-1} as the disk circular velocity, the $M_{\rm dyn} \sin^2 i$ will reduce from $2.4 \times 10^{11}\,M_\odot$ to $4.2 \times 10^{10}\,M_\odot$.

We then estimate the masses of the stellar components ($M_{\rm bulge}$) in the spheroidal bulges as $M_{\rm bulge} = M_{\rm dyn} - M_{\rm gas}$. We adopt a series of inclination angle values, i.e., $i = 1°$, 5°, 10°, 20°, 30°, 40°, 50°, 60°, and 90°, and derive $M_{\rm dyn}$ and $M_{\rm bulge}$ accordingly. The corresponding black hole–bulge mass ratios ($M_{\rm BH}/M_{\rm bulge}$) versus different inclination angles are plotted in Figure 7, compared to the local mass relationship of $M_{\rm BH} \sim 0.0014 M_{\rm bulge}$. The plot shows that if the sources were falling on the local black hole–bulge mass ratio of 0.0014 this would require inclination angles from <5° to ~25°, or <5° to 15° when the two broadest line objects are excluded.

However, the observed distribution of CO line widths of the $z \sim 6$ quasar sample is similar to that of the SMGs, which argues against systematically smaller inclination angle values. Moreover, these $z \sim 6$ quasars are all among the brightest objects in the quasar population with AGN bolometric luminosities of $L_{\rm bol} \geqslant 10^{13}\,L_\odot$. Recent studies showed that the unobscured fraction of quasars is increasing with quasar luminosity, and for objects with $L_{\rm bol} \geqslant 10^{13}\,L_\odot$, this fraction is probably larger than 50% (Simpson 2005; Treister et al. 2008). This is consistent with the receding torus model and implies a very large opening angle of the unobscured cone in these most

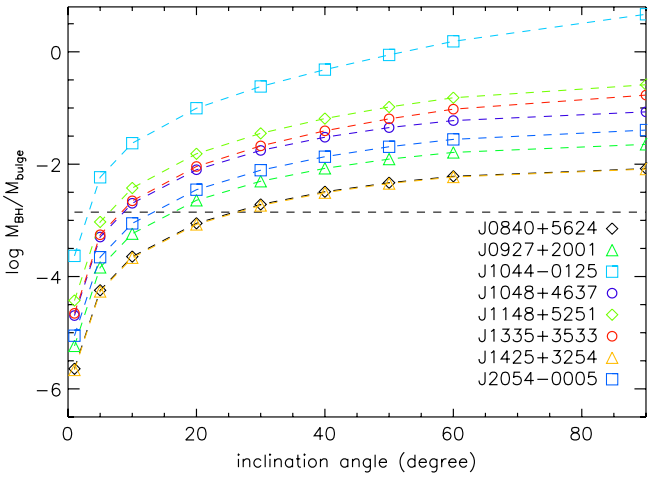

Figure 7. Derived ratios between the black hole and the bulge stellar masses vs. the inclination angles of the molecular disk. The bulge dynamical masses (M_{dyn} $\sin^2 i$) are derived using the CO FWHMs from single-Gaussian spectral fitting, and the bulge stellar masses (M_{bulge}) are estimated with $M_{dyn} - M_{gas}$. The plot shows how M_{BH}/M_{bulge} compares to present-day value of 0.0014 (dashed line) with different assumptions of inclination angles.

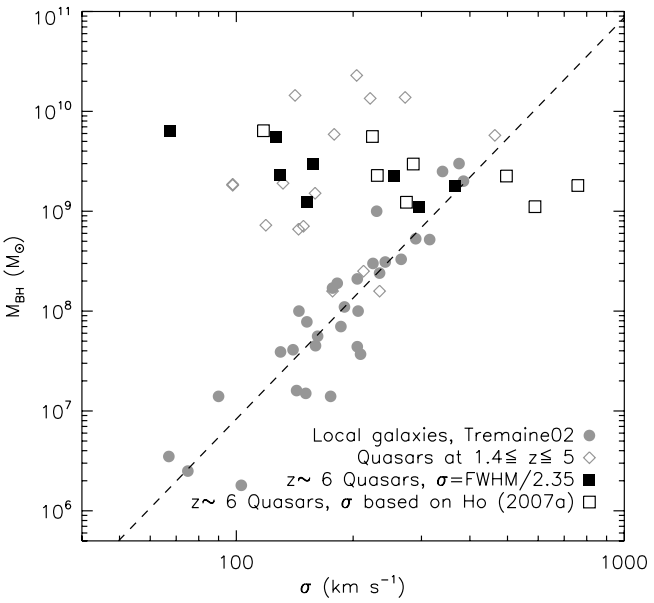

Figure 8. Black hole masses of the $z \sim 6$ quasars vs. their bulge velocity dispersion (σ). The dashed line denotes the local M_{BH}–σ relationship of $\log(M_{BH}/M_\odot) = 8.13 + 4.02\log(\sigma/200\,\mathrm{km\,s^{-1}})$ (Tremaine et al. 2002). The filled circles represent the local galaxies from Tremaine et al. (2002). The filled squares and open diamonds are for the $z \sim 6$ and $1.4 \leqslant z \leqslant 5$ quasar samples, respectively, with σ derived from the observed CO line width using $\sigma \approx$ FWHM/2.35. The open squares show the σ values derived with the method described in Ho (2007a) assuming an average inclination angle of 40° for the $z \sim 6$ quasars.

luminous quasars, i.e., the central AGNs can be directly seen over an inclination angel range of i from 0° to probably $\geqslant$60° (Elitzur 2008). Thus, though we cannot rule out small inclination angle values for individual objects, it is highly unlikely that more than half of these CO detected $z \sim 6$ quasars are viewed in the extreme inclination angle range of $i < 15°$. The CO estimated bulge dynamical masses probably reflect intrinsically smaller M_{BH}/M_{bulge} for these $z \sim 6$ quasars compared to that of the local mature galaxies.

We emphasize that accurate calculations of the bulge dynamical and stellar masses still require high-resolution measurements of the disk size and geometry for each object. To roughly constrain the average black hole–bulge mass ratio of these FIR and CO luminous $z \sim 6$ quasars here, we simply adopt an average inclination angle of 40° based on the assumption of uniformly distributed i between 0° and 60°. This results in a median M_{BH}/M_{bulge} ratio of 0.022 for our sample, which is about 15 times higher than the present-day value of 0.0014. This is in good agreement with the picture suggested by other high-z M_{BH}–M_{bulge} studies (e.g., Walter et al. 2004; Coppin et al. 2008a; Riechers et al. 2008a, 2008b; Peng et al. 2006a, 2006b), i.e., that the SMBH accumulates most its mass before the formation of the stellar bulge.

For further consideration, if these $z \sim 6$ quasars will finally evolve into systems with black hole–bulge relationships identical to that in the local universe, the final bulge stellar mass should be around 10^{12} $M_\odot$ with black hole masses on the order of 10^9 $M_\odot$. The M_{BH}/M_{bulge} ratio we derived above suggests that only $\lesssim$10% of the stellar component has been formed in these FIR and CO bright $z \sim 6$ quasars on the average. On the other hand, the detected molecular gas mass of $\sim 10^{10}$ $M_\odot$ in these objects can only account for $< 3\%$ of the mature bulge mass if the gas will all be converted to stars. Thus, large amounts of gas supplied from external sources is required to form the 10^{12} $M_\odot$ stellar bulge by $z = 0$.

5.2.2. M_{BH}–σ Relationship

We investigate the black hole mass–bulge velocity dispersion relation with the eight CO-detected $z \sim 6$ quasars in Figure 8. The SMBH mass (M_{BH}) and bulge velocity dispersion (σ) in local galaxies follow a relationship of $\log(M_{BH}/M_\odot) = 8.13 + 4.02\log(\sigma/200\,\mathrm{km\,s^{-1}})$ (Tremaine et al. 2002). We first roughly estimate σ for the eight $z \sim 6$ quasars with the CO line widths, using the empirical relation $\sigma \approx$ FWHM/2.35 (Shields et al. 2006; Nelson 2000). The results are plotted in Figure 8, together with the local active and inactive galaxies from Tremaine et al. (2002) and CO-detected $1.4 \leqslant z \leqslant 5$ quasars that have available SMBH mass measurements (Shields et al. 2006; Coppin et al. 2008a). Most of the high-z CO-detected quasars, especially the objects with $M_{BH} \geqslant 10^9$ $M_\odot$, are above the local M_{BH}–σ relationship with offsets of more than 1 order of magnitude in black hole mass, as was found in Shields et al. (2006). The median value of the ratios between M_{BH} and the expected black hole masses from the local M_{BH}–σ relation ($M_{BH,\sigma}$) for our $z \sim 6$ sample is $\langle M_{BH}/M_{BH,\sigma}\rangle_{median} \sim 40$.

This is consistent with the high M_{BH}/M_{bulge} ratios and the idea of prior SMBH formations we discussed in the previous section (Section 5.2.1). However, the systemic offset between the high-z objects and the local $M_{BH}-\sigma$ relation (i.e., $\langle M_{BH}/M_{BH,\sigma}\rangle_{median}$) can be reduced if we include assumptions of inclination angles in our estimations of σ, following the empirical correlations between σ and inclination angle-corrected CO line width from the literature (e.g., Ho 2007a, 2007b; Wu 2007). In particular, if we consider the possible gas disk inclination angle range for these $z \sim 6$ quasars and adopt an average value of $i = 40°$ (as was discussed in Section 5.2.1), the derived $\langle M_{BH}/M_{BH,\sigma}\rangle_{median}$ will reduce to $\sim$26 and 4 following the methods described in Wu (2007) and Ho (2007a), respectively.

We also note that our sample exhibits significant scatter on the M_{BH}–σ plot with derived $M_{BH}/M_{BH,\sigma}$ values over 3 orders of magnitude. This is mainly due to the intrinsic scatter and offset between the real bulge velocity dispersions and the CO estimated values based on the empirical relationships of low-z samples. Indeed, how the observed CO line widths trace the

bulge velocity dispersions in the high-z CO-detected quasars is still an open question. These objects are the most massive SMBH–host systems in the universe with SMBH masses of a few 10^9–$10^{10}\,M_\odot$ and experiencing massive star formation in the central kpc scale regions (Walter et al. 2009). We will expect the sensitive interferometer arrays (such as ALMA and the EVLA) to directly probe the gas properties, e.g., the gas distribution, geometry, dynamics (virialized or not), line profiles, and contributions from turbulence, etc., in their spheroidal hosts and finally address the $M_{\rm BH}$–σ correlation in these high-z FIR and CO luminous quasars.

6. CONCLUSIONS

We present new observations of molecular CO line emission and 350 μm dust continuum emission in quasar host galaxies at $z \sim 6$. Our most important finding is that high-order CO transitions are detected in all six of the $z \sim 6$ quasars observed with the 3 mm receiver on the PdBI. The new CO detections all have observed 250 GHz dust continuum flux densities of $S_{250\,\rm GHz} \geqslant 1.8$ mJy. These results, together with previous CO detections in another two objects, reveal an extremely high CO detection rate in the FIR luminous quasars at $z \sim 6$. With the final sample of eight CO-detected $z \sim 6$ quasars, we study the molecular gas properties in the earliest quasar host galaxies, and the main results are summarized as follows.

The CO emission indicates molecular gas masses of 0.7–$2.5 \times 10^{10}\,M_\odot$ in the quasar host galaxies. The observed CO line widths are spread over a wide range from 160 to 860 km s^{-1}, with a median value of about 360 km s^{-1}. The gas mass and CO line width distributions of the $z \sim 6$ quasars are consistent with samples of CO-observed SMGs and quasars at $1.4 \leqslant z \leqslant 5$.

The CO and FIR luminosities of the eight $z \sim 6$ quasars follow the $L_{\rm FIR}$–$L'_{\rm CO}$ relationship derived for local spirals, LIRGs, ULIRGs, high-z SMGs, and CO-detected quasars, though the weakest CO detection has the largest offset from the trend. This is consistent with the idea of coeval star formation with rapid growth of the SMBH in the early quasar–host systems. The derived SFRs are from ~530 to 2380 $M_\odot$ yr^{-1}. The corresponding star formation efficiencies indicated by the ratios of SFR/$M_{\rm gas}$ are consistent with the extreme starburst systems at low and high redshifts.

We investigate the black hole–bulge correlations of these FIR and CO luminous quasars at $z \sim 6$ using the CO measurements. Based on certain assumptions of the molecular gas disk size, average inclination angle, and σ–CO line width relation, we estimate the bulge dynamical masses and velocity dispersions for our sample and compare them to the local black hole–bulge relationships. The results suggest that the black hole masses of these $z \sim 6$ quasars are typically an order of magnitude higher than the values expected from the present-day relationships, which is consistent with the idea that the formation of the SMBHs occurs prior to that of the stellar bulges in the massive high-z quasar–galaxy systems. However, we also recognize that there are large uncertainties in the estimations of $M_{\rm bulge}$ and σ for individual objects due to unknown gas distribution, disk inclination, and dynamics. Further high-resolution observations of quasar host galaxies should focus on these FIR and CO luminous $z \sim 6$ quasars to fully understand the black hole-bulge evolution at the highest redshift.

This work is based on observations carried out with the IRAM PdBI, the GBT (NRAO), the VLA (NRAO), and the SHARC-II bolometer camera at the CSO. IRAM is supported by INSU/CNRS (France), MPG (Germany), and IGN (Spain). The CSO is supported by the NSF under AST-0540882. The National Radio Astronomy Observatory (NRAO) is a facility of the National Science Foundation operated under cooperative agreement by Associated Universities, Inc. We thank the anonymous referee for useful comments. R.W. thanks Dr. Alexandre Beelen at Institut d'Astrophysique Spatiale for helpful discussions and suggestions. We acknowledge support from the Max-Planck Society and the Alexander von Humboldt Foundation through the Max-Planck-Forschungspreis 2005. D.A.R. acknowledges support from NASA through Hubble Fellowship grant HST-HF-51235.01 awarded by the Space Telescope Science Institute, which is operated by the Association of Universities for Research in Astronomy, Inc., for NASA, under contract NAS 5-26555. R.W. acknowledges support of the National Natural Science Foundation of China grant 10833006 and grant 0816341034.

Facilities: IRAM:30m (MAMBO), VLA, Sloan (SDSS) CSO (SHARC-II), GBT

REFERENCES

Beelen, A., Cox, P., Benford, D. J., Dowell, C. D., Kovács, A., Bertoldi, F., Omont, A., & Carilli, C. L. 2006, ApJ, 642, 694
Benford, D. J., Cox, P., Omont, A., Phillips, T. G., & McMahon, R. G. 1999, ApJ, 518, L65
Bertoldi, F., Carilli, C. L., Cox, P., Fan, X., Strauss, M. A., Beelen, A., Omont, A., & Zylka, R. 2003a, A&A, 406, L55
Bertoldi, F., et al. 2003b, A&A, 409, L47
Brown, R. L., & Vanden Bout, P. A. 1992, ApJ, 397, L19
Carilli, C. L., & Wang, R. 2006, AJ, 131, 2763
Carilli, C. L., et al. 2002, AJ, 123, 1838
Carilli, C. L., et al. 2004, AJ, 128, 997
Carilli, C. L., et al. 2007, ApJ, 666, L9
Chapman, S. C., Blain, A. W., Smail, I., & Ivison, R. J. 2005, ApJ, 622, 772
Cool, R. J., et al. 2006, AJ, 132, 823
Coppin, K. E. K., et al. 2008a, MNRAS, 389, 45
Coppin, K. E. K., et al. 2008b, MNRAS, 384, 1597
Cox, P., et al. 2002, A&A, 387, 406
Daddi, E., Dannerbauer, H., Elbaz, D., Dickinson, M., Morrison, G., Stern, D., & Ravindranath, S. 2008, ApJ, 673, L21
Daddi, E., et al. 2010, ApJ, in press (arXiv:0911.2776)
Downes, D., & Solomon, P. M. 1998, ApJ, 507, 615
Elitzur, M. 2008, New Astron. Rev, 52, 274
Elvis, M., et al. 1994, ApJS, 95, 1
Fan, X., Carilli, C. L., & Keating, B. 2006a, ARA&A, 44, 415
Fan, X., et al. 2000, AJ, 120, 1167
Fan, X., et al. 2003, AJ, 125, 1649
Fan, X., et al. 2006b, AJ, 131, 1203
Fan, X., et al. 2006c, AJ, 132, 117
Fixsen, D. J., Bennett, C. L., & Mather, J. C. 1999, ApJ, 526, 207
Freudling, W., Corbin, M. R., & Korista, K. T. 2003, ApJ, 587, L67
Gao, Y., & Solomon, P. M. 2004, ApJS, 152, 63
Goodrich, R. W., et al. 2001, ApJ, 561, L23
Greve, T. R., et al. 2005, MNRAS, 359, 1165
Guilloteau, S., & Lucas, R. 2000, in ASP Conf. Ser. 217, Imaging at Radio through Submillimeter Wavelengths, ed. J. G. Mangum & S. J. E. Radford (San Francisco, CA: ASP), 299
Ho, L. C. 2007a, ApJ, 669, 821
Ho, L. C. 2007b, ApJ, 668, 94
Hopkins, P. F., Hernquist, L., Cox, T. J., Robertson, B., & Krause, E. 2007a, ApJ, 669, 67
Hopkins, P. F., Hernquist, L., Cox, T. J., Robertson, B., & Krause, E. 2007b, ApJ, 669, 45
Isobe, T., Feigelson, E. D., Akritas, M. G., & Babu, G. J. 1990, ApJ, 364, 104
Iwamuro, F., Kimura, M., Eto, S., Maihara, T., Motohara, K., Yoshii, Y., & Doi, M. 2004, ApJ, 614, 69
Jiang, L., et al. 2006, AJ, 132, 2127
Jiang, L., et al. 2007, AJ, 134, 1150
Jiang, L., et al. 2008, AJ, 135, 1057
Kauffmann, G., & Haehnelt, M. 2000, MNRAS, 311, 576
Kennicutt, R. C. 1998, ARA&A, 36, 189

Kreysa, E., et al. 1998, Proc. SPIE, 3357, 319
Kovács, A. 2006, PhD thesis, Caltech
Kovács, A., Chapman, S. C., Dowell, C. D., Blain, A. W., Ivison, R. J., Smail, I., & Phillips, T. G. 2006, ApJ, 650, 592
Maiolino, R., Oliva, E., Ghinassi, F., Pedani, M., Mannucci, F., Mujica, R., & Juarez, Y. 2004a, A&A, 420, 889
Maiolino, R., Schneider, R., Oliva, E., Bianchi, S., Ferrara, A., Mannucci, F., Pedani, M., & Roca Sogorb, M. 2004b, Nature, 431, 533
Maiolino, R., et al. 2007, A&A, 472, L33
Marconi, A., & Hunt, L. K. 2003, ApJ, 589, L21
Narayanan, D., et al. 2008, ApJS, 174, 13
Nelson, C. H. 2000, ApJ, 544, L91
Neri, R., et al. 2003, ApJ, 597, L113
Omont, A., Beelen, A., Bertoldi, F., McMahon, R. G., Carilli, C. L., & Isaak, K. G. 2003, A&A, 398, 857
Omont, A., McMahon, R. G., Cox, P., Kreysa, E., Bergeron, J., Pajot, F., & Storrie-Lombardi, L. J. 1996a, A&A, 315, 1
Omont, A., et al. 1996b, Nature, 382, 428
Peng, C. Y., Impey, C. D., Ho, L. C., Barton, E. J., & Rix, H.-W. 2006a, ApJ, 640, 114
Peng, C. Y., Impey, C. D., Rix, H.-W., Kochaneck, C. S., Keeton, C. R., Falco, E. E., Lehár, J., & McLeod, B. A. 2006b, ApJ, 649, 616
Petric, A. O., Carilli, C. L., Bertoldi, F., Fan, X., Cox, P., Strauss, M. A., Omont, A., & Schneider, D. P. 2003, AJ, 126, 15
Priddey, R. S., Isaak, K. G., McMahon, R. G., Roboson, E. I., & Pearson, C. P. 2003, MNRAS, 344, L74
Richards, G. T., Vanden Berk, D. E., Reichard, T. A., Hall, P. B., Schneider, D. P., SubbaRao, M., Thakar, A. R., & York, D. G. 2002, AJ, 124, 1
Riechers, D. A., Walter, F., Brewer, B. J., Carilli, C. L., Lewis, G. F., Bertoldi, F., & Cox, P. 2008a, ApJ, 686, 851
Riechers, D. A., Walter, F., Carilli, C. L., & Bertoldi, F. 2007, ApJ, 671, L13
Riechers, D. A., Walter, F., Carilli, C. L., Bertoldi, F., & Momjian, E. 2008b, ApJ, 686, L9
Riechers, D. A., et al. 2006, ApJ, 650, 604
Riechers, D. A., et al. 2009, ApJ, 703, 1338
Robson, I., Priddey, R. S., Isaak, K. G., & McMahon, R. G. 2004, MNRAS, 351, L29
Ryan-Weber, E. V., Pettini, M., Madau, P., & Zych, B. J. 2009, MNRAS, 395, 1476
Seaquist, E. R., Ivison, R. J., & Hall, P. J. 1995, MNRAS, 276, 867
Shields, G. A., Menezes, K. L., Massart, C. A., & Vanden Bout, P. 2006, ApJ, 641, 683
Simpson, C. 2005, MNRAS, 360, 565
Smail, I., Ivison, R. J., Blain, A. W., & Kneib, J.-P. 2002, MNRAS, 331, 495
Solomon, P. M., Downes, D., Radford, S. J. E., & Barrett, J. W. 1997, ApJ, 478, 144
Solomon, P. M., & Vanden Bout, P. A. 2005, ARA&A, 43, 677 (SV05)
Spergel, D. N., et al. 2007, ApJS, 170, 377
Tacconi, L. J., et al. 2006, ApJ, 640, 228
Treister, E., Krolik, J. H., & Dullemond, C. 2008, ApJ, 679, 140
Tremaine, S., et al. 2002, ApJ, 574, 740
Wagg, J., Hughes, D. H., Aretxaga, I., Chapin, E. L., Dunlop, J. S., Gaztañaga, E., & Devlin, M. 2007, MNRAS, 375, 745
Wagg, J., Wang, R., Carilli, C., Walter, F., Maddalena, R., & Pisano, D. J. 2008, GBT Memo 256
Walter, F., Carilli, C. L., Bertoldi, F., Menten, K., Cox, P., Lo, K. Y., Fan, X., & Strauss, M. A. 2004, ApJ, 615, L17
Walter, F., Riechers, D., Cox, P., Neri, R., Carilli, C., Bertoldi, F., Weiß, A., & Maiolino, R. 2009, Nature, 457, 699
Walter, F., et al. 2003, Nature, 424, 406
Wang, R., et al. 2007, AJ, 134, 617
Wang, R., et al. 2008a, AJ, 135, 1201
Wang, R., et al. 2008b, ApJ, 687, 848
Weiß, A., Downes, D., Walter, F., & Henkel, C. 2005a, A&A, 440, L45
Weiß, A., Walter, F., & Scoville, N. Z. 2005b, A&A, 438, 533
Weiß, A., et al. 2007, A&A, 467, 955
Willott, C. J., McLure, R. J., & Jarvis, M. J. 2003, ApJ, 587, L15
Willott, C. J., et al. 2007, AJ, 134, 2435
Willott, C. J., et al. 2009a, AJ, 137, 3541
Willott, C. J., et al. 2009b, AJ, in press (arXiv:0912.0281)
Wu, X.-B. 2007, ApJ, 657, 177